

Convection in porous media with dispersion

Baole Wen,^{1,2,*} Kyung Won Chang,^{2,†} and Marc A. Hesse^{1,2,‡}

¹*Institute of Computational Engineering and Sciences,
The University of Texas at Austin, Austin, TX 78712 USA*

²*Department of Geological Sciences, Jackson School of Geosciences,
The University of Texas at Austin, Austin, TX 78712 USA*

We investigate the effect of dispersion on convection in porous media by performing direct numerical simulations (DNS) in a two-dimensional Rayleigh-Darcy domain. Scaling analysis of the governing equations shows that the dynamics of this system are not only controlled by the classical Rayleigh-Darcy number based on molecular diffusion, Ra_m , and the domain aspect ratio, but also controlled by two other dimensionless parameters: the dispersive Rayleigh number $Ra_d = H/\alpha_t$ and the dispersivity ratio $r = \alpha_l/\alpha_t$, where H is the domain height, α_t and α_l are the transverse and longitudinal dispersivities, respectively. For $\Delta = Ra_d/Ra_m > O(1)$, the influence from the mechanical dispersion is minor; for $\Delta \ll 1$, however, the flow pattern is controlled by Ra_d while the convective flux is $F \sim Ra_m$ for large Ra_m , but with a prefactor that has a non-monotonic dependence on Ra_d . Our DNS results also show that the increase of mechanical dispersion, i.e. decreasing Ra_d , will coarsen the convective pattern by increasing the plume spacing. Moreover, the inherent anisotropy of mechanical dispersion breaks the columnar structure of the mega-plumes at large Ra_m , if $Ra_d < 5000$. This results in a fan-flow geometry that reduces the convective flux.

Convection in porous media controls mass and energy transfer in many natural and engineered applications [1–4]. This subject has received renewed interest due to its potential impact on geological carbon dioxide (CO₂) storage, which allows large reductions of CO₂ emissions from fossil fuel-based electricity generation [5–7]. After the CO₂ is injected into the deep saline aquifers, it dissolves into the brine and increases the brine density. The dissolution of CO₂ eventually forms a stable stratification and ensures secure long-term storage [8, 9].

The rate of CO₂ dissolution is limited by mass transfer of dissolved CO₂ away from the CO₂-brine interface. Diffusive mass transport may take millions of years to saturate the brine [10–12]. However, once the diffusive boundary layer of dissolved CO₂ in brine has grown thick enough, it might become unstable and subsequently, convection sets in and forms descending CO₂-rich plumes. This process greatly increases the CO₂ dissolution rate and significantly reduces the leakage risk of buoyant CO₂ into potable aquifers or into the atmosphere [13].

Dynamics of porous media convection can be studied in either a ‘one-sided’ system where convection is driven by a source of buoyancy on only one boundary, e.g. the solutal convection system [14–19], or a ‘two-sided’ system where both of top and bottom boundaries actively drive the convection, e.g. the thermal convection system [16, 20–25]. These two systems share many common characteristics in convective pattern and transport properties, although dynamics in the former generally evolve over time while there exists a statistically-steady state in the later. In this study, we focus on the two-sided convective system to perform long-time direct numerical simulations (DNS) for reliable statistically results.

In the absence of mechanical dispersion, the flow pattern and transport flux of convection in porous media

are generally thought to be controlled by the molecular Rayleigh number,

$$Ra_m = \frac{k\Delta\rho gH}{\mu\phi D_m}, \quad (1)$$

where k is the medium permeability, $\Delta\rho$ the density change between the fresh and the saturated water, g the acceleration of gravity, H the domain height, μ the dynamic viscosity of the fluid, ϕ the porosity, and D_m the molecular diffusion coefficient. At large Ra_m , convection appears in the form of columnar plumes fed continually with a series of proto-plumes generated from the diffusive boundary layer. As Ra_m is increased, the inter-plume spacing δ and the flux F in the quasi-steady convective regime follow specific power-law scalings of Ra_m , i.e. $\delta \sim Ra_m^{-\alpha}$ with the positive exponent $\alpha \leq 0.5$ [16, 22, 23, 26–28], and $F \sim Ra_m^\beta$ with $\beta = 1$ reported by [18, 21, 22, 27–32], although experimental results have been interpreted to suggest lower exponents $0.8 \leq \beta < 1$ [15, 33].

However, recent bench-top experiments on solutal convection in porous media show that Ra_m does not control the convective pattern in typical granular media, because mechanical dispersion is the dominant dissipative mechanism [34]. Mechanical dispersion in porous media is due to non-uniformities in the flow that cause mixing of the solute [35–37]. In an isotropic and homogeneous porous medium, mechanical dispersion is described by two parameters: the longitudinal and transverse dispersivities α_l and α_t , respectively [38–40]. Therefore, the hydrodynamic dispersion tensor in the fixed Cartesian reference frame can be expressed as

$$\mathbf{D}^* = D_m \mathbf{I} + (\alpha_l - \alpha_t) \frac{\mathbf{u}^* \mathbf{u}^*}{|\mathbf{u}^*|} + \alpha_t |\mathbf{u}^*| \mathbf{I}, \quad (2)$$

where \mathbf{I} denotes the identity matrix and the mechanical

dispersion scales linearly with the interstitial fluid velocity \mathbf{u}^* . As long as $|\mathbf{u}^*| \ll D_m/\alpha_l$, $\mathbf{D}^* \approx D_m \mathbf{I}$, so that molecular diffusion dominates over hydrodynamic dispersion; when $|\mathbf{u}^*| \gg D_m/\alpha_l$, however, the mechanical dispersion starts to dominate.

Recent studies by [34, 41–46] indicate that hydrodynamic dispersion significantly affects the flow pattern and mass transport of convection in porous media at large Ra_m . The numerical simulations by [42, 43] show that hydrodynamic dispersion enhances the convective mixing and greatly reduces the onset time for convection; however, the experiments by [34, 45] reveal that the mechanical dispersion coarsens the convective pattern and reduces the increase of convective flux with increasing permeability k . Particularly, the systematic experiments by [34] illustrate that adjusting Ra_m via changing the density difference $\Delta\rho$ or the medium permeability k may result in distinct convective characteristics due to hydrodynamic dispersion. For fixed $\Delta\rho$, increasing k (via choosing a larger glass bead diameter d as $k \sim d^2$) raises Ra_m but *enlarges* the inter-plume spacing δ ; for fixed k , however, δ is nearly fixed for increasing $\Delta\rho$. Secondly, for fixed $\Delta\rho$, the dissolution flux F does not increase linearly with k and is lower than expected at high k ; for fixed k , in contrast, $F \sim cRa_m^1$ with decreasing prefactor c as k is increased. Nevertheless, the vertical velocity, via measuring the speed of the fastest descending fingertip, approximately increases linearly with both $\Delta\rho$ and k . Some of the above findings contradict the classical predictions made in the absence of mechanical dispersion.

To understand the effect of dispersion on convection, we perform DNS in a two-dimensional (2D), rectangular, homogeneous and isotropic Rayleigh-Darcy domain. We aim to identify the dimensionless parameters governing convection in porous media with hydrodynamic dispersion, determine the scaling law for the quasi-steady convective flux, and quantify the contribution of molecular diffusion and mechanical dispersion to the hydrodynamic dissipation. As mentioned earlier, we focus on a two-sided convective system for long-time statistical results.

In previous studies, the dispersivity, α_l or α_t , and the molecular diffusivity D_m are combined to define the characteristic length and time scales or the Rayleigh number [42, 43]. In this work, however, we rescale the system using the domain height H , the buoyancy velocity $U = k\Delta\rho g/(\mu\phi)$, and the convective timescale $T_c = H/U$. We show below that this allows us to decouple the parameters controlling the flow pattern and the flux which simplifies the discussion. Based on these scales, we obtain the dimensionless equations

$$\frac{\partial C}{\partial t} + \mathbf{u} \cdot \nabla C = \nabla \cdot (\mathbf{D} \nabla C), \quad (3a)$$

$$\mathbf{u} = -\nabla p - C \mathbf{e}_z, \quad (3b)$$

$$\nabla \cdot \mathbf{u} = 0, \quad (3c)$$

where C , $\mathbf{u} = (u, w)$, and p are the dimensionless forms

of concentration, velocity, and pressure, respectively, and \mathbf{e}_z is a unit vector in z (upward) direction. The dimensionless hydrodynamic dispersion tensor is then given by

$$\mathbf{D} = Ra_m^{-1} \mathbf{I} + Ra_d^{-1} \left[(r-1) \frac{\mathbf{u}\mathbf{u}}{|\mathbf{u}|} + |\mathbf{u}| \mathbf{I} \right], \quad (4)$$

and characterized by the molecular Rayleigh number Ra_m defined in (1) and two additional parameters,

$$Ra_d = \frac{H}{\alpha_t} \quad \text{and} \quad r = \frac{\alpha_l}{\alpha_t}, \quad (5a,b)$$

which are referred to as dispersive Rayleigh number and dispersivity ratio, respectively. The dissipation by mechanical dispersion increases with decreasing Ra_d .

The flow is assumed to be periodic laterally with an impermeable top and bottom boundaries. Solute concentration along the top and bottom boundaries is unity and null, respectively. Hence, the boundary conditions at the top and the bottom are given by

$$C|_{z=1} = 1 \quad \text{and} \quad w|_{z=1} = 0; \quad C|_{z=0} = w|_{z=0} = 0. \quad (6)$$

Note that the problem posed by (3) and (6) is formally identical to the two-sided thermal convection problem in which the domain is heated from below and cooled from above. Here, (3) and (6) are solved numerically using a Fourier-Chebyshev-tau pseudospectral solver developed in [27, 28], the temporal discretization is achieved using a three-step semi-implicit Runge-Kutta scheme [47], and the numerical scheme is parallelized using the Message Passing Interface (MPI). In order to obtain reliable statistical results, the DNS are performed up to $O(10^3)$ convective time units. As the transverse dispersivity is usually an order of magnitude less than the longitudinal dispersivity [48–50], we set $r = 10$ in all simulations.

To quantify the flow, we measure the convective flux F at the top wall,

$$F = \left\langle \frac{\partial C}{\partial z} + \frac{Ra_m}{Ra_d} \overline{|u| \frac{\partial C}{\partial z}} \right\rangle_{z=1} = F_m + F_d, \quad (7)$$

where the angle bracket and the overbar denote the long-time and the horizontal averages, respectively, the first term on the right side of (7) represents the flux at the boundary via pure molecular diffusion F_m , and the second term represents the flux via mechanical dispersion F_d . We also measure the inter-plume spacing δ by time-averaging the dominant Fourier mode number at the interior, the mean horizontal velocity at the top wall, $\tilde{u} = \langle \overline{|u|} \rangle_{z=1}$, the mean vertical velocity at the interior, $\tilde{w} = \langle \overline{|w|} \rangle_{z=\frac{1}{2}}$, and the magnitude of the time-averaged w extremum value at the interior, $w_m = \langle \max(|w|_{z=\frac{1}{2}}) \rangle$.

Figures 1 and 2 show the variation of the convective flow pattern and the corresponding statistical DNS results as a function of Ra_d for $Ra_m = 20000$. When the smallest diffusive length scale $1/Ra_m$ is much larger than the pore scale of the medium d/H , i.e. $Ra_d \gg rRa_m$

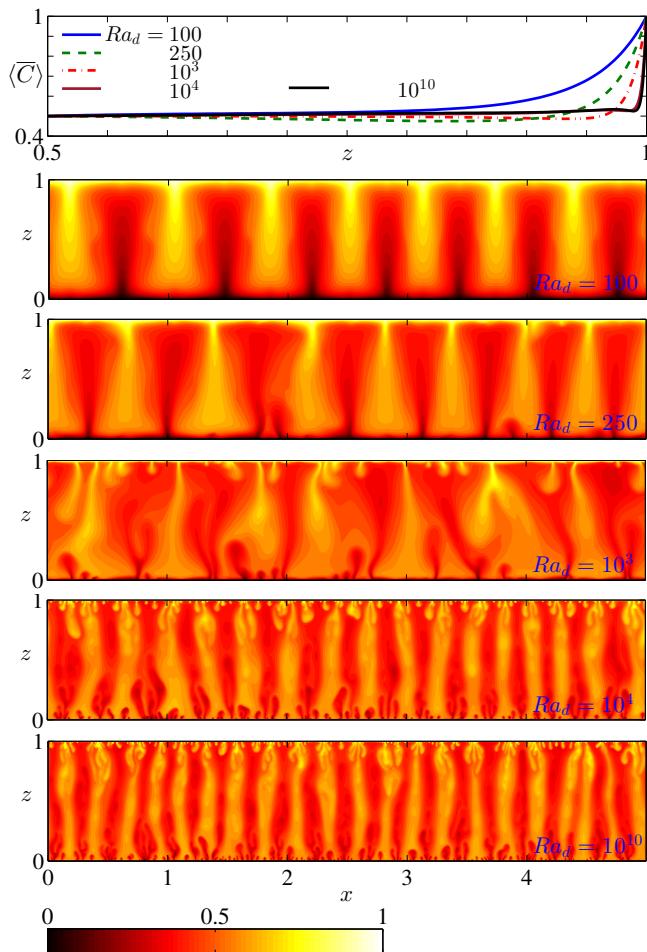


FIG. 1. Time-averaged horizontal-mean concentration profile $\langle \bar{C} \rangle$ and snapshots of the concentration field C from DNS at $Ra_m = 20000$ and $r = 10$ for different Ra_d . The domain aspect ratio is $L = 5$.

as $\alpha_t \approx d/r$ [36, 51], the molecular diffusion dominates the hydrodynamics dispersion [18, 22, 34]. Our DNS results reveal that only for $\Delta \equiv Ra_d/Ra_m \gtrsim 10^5$, the mechanical dispersion can be completely negligible so that the convection converges to the classical columnar flow [21, 22, 27]. When $O(1) < \Delta < 10^5$, the relatively weak mechanical dispersion slightly enhances the convective transport but the flow still retains the columnar structure. For $\Delta < O(1)$, however, the mechanical dispersion starts to apparently affect the convective pattern and flux: the convection transitions to a fan flow with laterally expanding mega-plumes along the vertical flow direction, and the convective flux is reduced to approximately 50% of the high- Ra_d value at $\Delta = 0.05$.

Increasing dispersion thickens the diffusive boundary layer, smooths the small-scale plumes near the walls, and stabilizes the flow. Eventually, the convection becomes steady at $Ra_d = 100$ (Fig. 1) and the flux is again in-

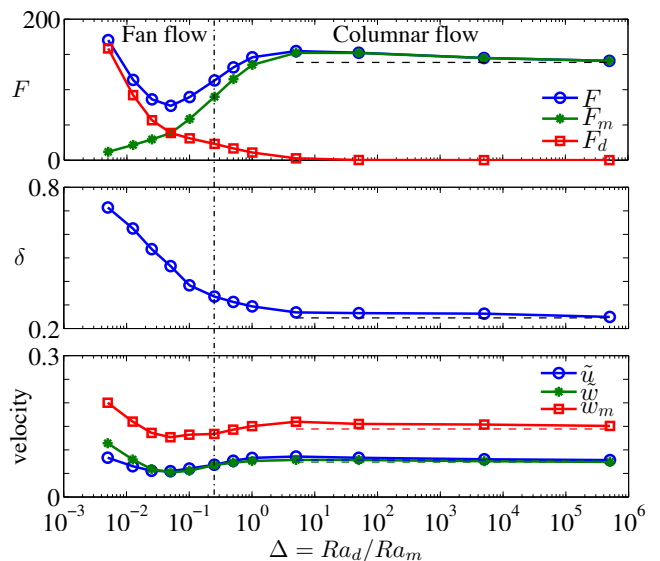


FIG. 2. Statistical DNS results of convection at $Ra_m = 20000$ and $r = 10$ for different Ra_d . The domain aspect ratio is $L = 5$. The dashed lines denote the results in the absence of mechanical dispersion and the dashed-dot line separates the fan-flow and the columnar-flow regions.

creased for $\Delta \leq 0.05$ due to the large magnitude of the effective diffusion coefficient induced by the mechanical dispersion. Moreover, it is also seen from Fig. 2 that the hydrodynamic dispersion coarsens the flow pattern by increasing δ , and the mean buoyancy velocities at the top and the interior, \tilde{u} , \tilde{w} and w_m , roughly follow the same trend with the convective flux as a function of Ra_d . It should be noted that the w extremum value, w_m , becomes nearly constant for $0.025 \leq \Delta \leq 0.25$.

Figures 3 and 4 show the convective pattern and the corresponding statistical DNS results as a function of Ra_m for $Ra_d = 1000$. The convection basically remains a fan-flow structure at $Ra_d = 1000$ as $Ra_m \rightarrow \infty$. In particular, the inter-plume spacing δ is nearly invariant when $\Delta \lesssim 0.2$; the mean velocities \tilde{u} and \tilde{w} are roughly unchanged after $\Delta \lesssim 0.05$; and the horizontal-mean concentration profile \bar{C} becomes almost fixed for $\Delta \lesssim 0.02$, so that at the top and the bottom, the flux due to molecular diffusion (i.e. F_m) levels off. In short, at sufficiently large Ra_m , the flow pattern and the statistical system quantities (i.e. \bar{C} , δ , \tilde{u} , \tilde{w} and w_m) are independent of Ra_m . Actually, as $Ra_m \rightarrow \infty$, the hydrodynamic dispersion tensor (4) reduces to

$$\mathbf{D} \rightarrow Ra_d^{-1} \left[(r-1) \frac{\mathbf{u}\mathbf{u}}{|\mathbf{u}|} + |\mathbf{u}|\mathbf{I} \right], \quad (8)$$

so that Ra_d becomes the only parameter controlling the dynamics of the system (for fixed r). Thus, at large Ra_m the concentration field C and the buoyancy velocity \mathbf{u} are determined by the dispersive Rayleigh number Ra_d ,

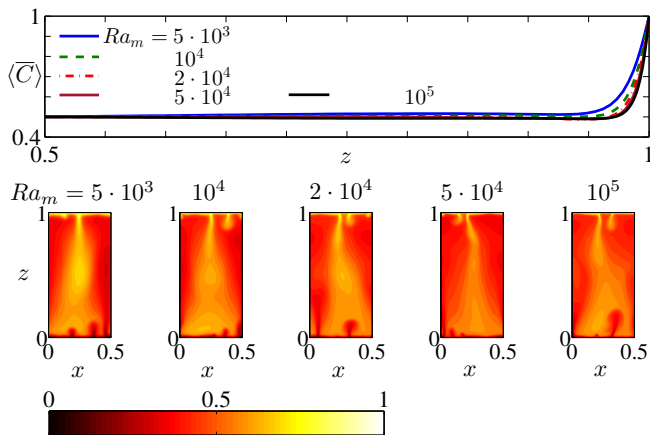


FIG. 3. Time-averaged horizontal-mean concentration profile $\langle C \rangle$ and snapshots of the concentration field C from DNS at $Ra_d = 1000$ and $r = 10$ for different Ra_m . For $Ra_m \leq 20000$, the domain aspect ratio is $L = 5$; while for $Ra_m > 20000$, DNS are performed in a small unit $L = 0.5$ where there only exists a single rising and descending mega-plume but the turbulent convection still sustains itself.

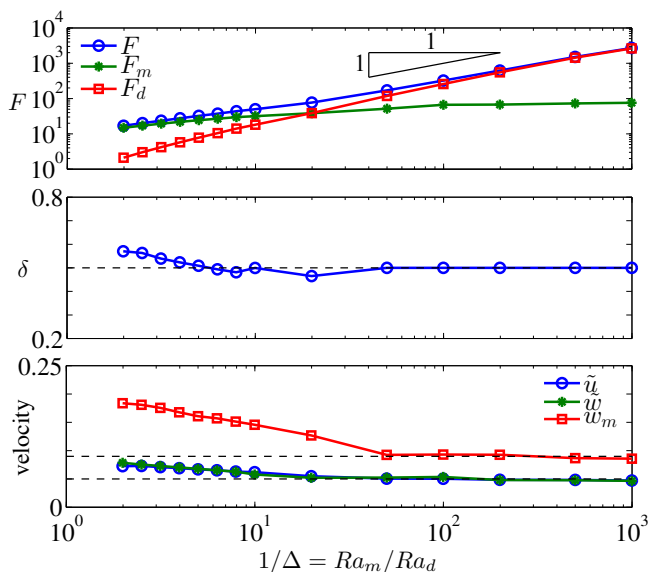


FIG. 4. Statistical DNS results of convection at $Ra_d = 1000$ and $r = 10$ for different Ra_m . L is as in Fig. 3.

as confirmed by our DNS data. Once C and \mathbf{u} become invariant in the limit of $Ra_m \rightarrow \infty$, $F_m \sim c_1$ and $F_d \sim c_2 \cdot Ra_m^1$ with the constants c_1 and c_2 determined by Ra_d .

A natural question concerns how the mechanical dispersion affects convection in the (Ra_m, Ra_d) parameter space. For $\Delta > O(1)$, the influence from the mechanical dispersion is minor, so that both the convective pattern and flux are controlled by Ra_m ; for $0.02 \lesssim \Delta < O(1)$, both the molecular diffusion and the mechanical disper-

sion are important to convection, e.g. they equally affect the flux at $\Delta \approx 0.05$; for $\Delta < 0.02$, the mechanical dispersion dominates the hydrodynamic dispersion: the flow pattern is determined by Ra_d , e.g. $C = C(Ra_d)$, $\delta = \delta(Ra_d)$ and $\mathbf{u} = \mathbf{u}(Ra_d)$, while the flux is predominantly controlled by Ra_m , e.g. $F \sim c_2(Ra_d) \cdot Ra_m^1$.

Below we apply these results to the recent laboratory experiments on solutal convection in porous media [34]. In granular media, the mechanical dispersion is proportional to grain size, $\alpha_l \sim d$, so that the appropriate dispersive Rayleigh number is $Ra_d \approx rH/d$ [36, 51]. Hence, increasing the grain size from 0.8 mm to 4 mm simultaneously increases Ra_m from $1.4 \cdot 10^4$ to $5.0 \cdot 10^5$ ($\Delta\rho = 9.3$ kg/m³) but decreases Ra_d from 3750 to 750, thereby reducing Δ from 0.3 to $1.5 \cdot 10^{-3}$. For $\Delta < 0.02$, the mechanical dispersion dominates the hydrodynamic dispersion and determines the convective pattern. Therefore, increasing the grain size at fixed $\Delta\rho$ intensifies the mechanical dispersion and coarsens the convective pattern. On the other hand, varying $\Delta\rho$ at fixed k only changes Ra_m and does not affect the flow pattern set by Ra_d .

Moreover, for fixed d , the prefactor $c_2(Ra_d)$ is constant so that the convective flux, $F \sim c_2 \cdot Ra_m^1$, increases linearly with $\Delta\rho$; while for fixed $\Delta\rho$, F is lower than expected at higher k since the pattern transitions from columnar flow to fan flow as Ra_d declines (Fig. 2). However, this reduction in F is accompanied only by a slight reduction in w_m (Fig. 2), which is consistent with the experimental observation that the speed of the fastest fingers increases approximately linearly with both $\Delta\rho$ and k [34].

Our DNS results and analysis above reveal that at sufficiently large Ra_m , the convective pattern is determined by the dispersive Rayleigh number Ra_d : the convection appears in the form of columnar flow at $Ra_d \geq 5000$ and then transitions to a fan flow at $Ra_d < 5000$. Although the convection also exhibits a fan-flow structure at small and moderate Ra_m in the absence of mechanical dispersion [20, 21], the physics are different. The fan-flow structure here is due to the inherent anisotropy of mechanical dispersion. As shown in Fig. 5, near the top and the bottom walls the flow between the neighboring plumes is dominantly horizontal, so the inter-plume spacing is set by the lateral dispersion $D_{xx}^w \approx D_m + \alpha_l u^w$ and the thickness of the diffusive boundary layer is significantly affected by the vertical dispersion $D_{zz}^w \approx D_m + \alpha_t u^w$. At the roots of the plumes, however, the flow is dominantly vertical, so the plume width is controlled by the lateral dispersion $D_{xx}^r \approx D_m + \alpha_t w^r$. The mass conservation of the incompressible flow requires $u^w \approx w^r$ near the wall. Hence, the inherent anisotropy of the mechanical dispersion, $r \gg 1$, leads to $D_{xx}^w \gg D_{xx}^r$, and thereby the increment of the inter-plume spacing is much larger than that of the plume width. This asymmetry results in the fan-flow structure and reduces the transport efficiency.

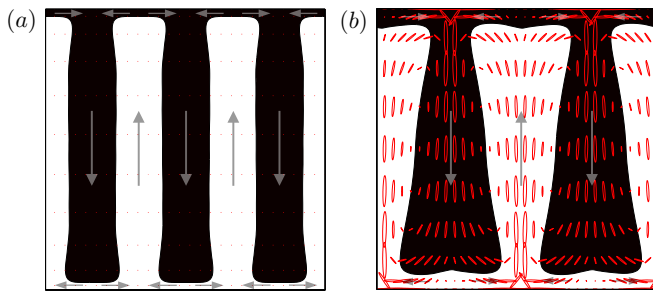


FIG. 5. Schematics showing the distribution of the hydrodynamic dispersion tensor in the form of ellipse. (a): columnar flow in the absence of mechanical dispersion; (b): fan flow with mechanical dispersion. In (a), $\mathbf{D}^* = D_m \mathbf{I}$ is homogeneous and isotropic; in (b), the anisotropy of the hydrodynamic dispersion leads to an asymmetry between the rising and the descending mega-plumes near the walls.

* wenbaole@gmail.com or baole@ices.utexas.edu

† Present address: Geomechanics Department, Sandia National Laboratories, Albuquerque, NM 87123 USA

‡ mhesse@jsg.utexas.edu

- [1] C. W. Horton and F. T. Rogers, *J. Appl. Phys.* **16**, 367 (1945).
- [2] E. R. Lapwood, *Proc. Camb. Phil. Soc.* **44**, 508 (1948).
- [3] O. M. Phillips, *Geological Fluid Dynamics: Sub-surface Flow and Reactions* (Cambridge University Press, 2009).
- [4] D. A. Nield and A. Bejan, *Convection in Porous Media*, 3rd ed. (Springer, New York, 2006).
- [5] F. Orr, *Science* **325**, 1656 (2009).
- [6] K. Michael, A. Golab, V. Shulakova, J. Ennis-King, G. Allinson, S. Sharma, and T. Aiken, *International Journal of Greenhouse Gas Control* **4**, 659 (2010).
- [7] M. L. Szulczewski, C. W. MacMinn, H. J. Herzog, and R. Juanes, *PNAS* **109**, 5185 (2012).
- [8] G. Weir, S. White, and W. Kissling, *Transport in Porous Media* **23**, 61 (1996).
- [9] J. P. Ennis-King and L. Paterson, *SPE Journal* **10**, 349 (2005).
- [10] K. Sathaye, M. Hesse, M. Cassidy, and D. Stockli, *PNAS* **111**, 15332 (2014).
- [11] D. Akhbari and M. A. Hesse, *Geology* **45**, 47 (2017).
- [12] B. Wen, D. Akhbari, L. Zhang, and M. A. Hesse, in revision for *J. Fluid Mech.* (arXiv:1801.02537) (2018).
- [13] J. J. Roberts, R. A. Wood, and R. S. Haszeldine, *PNAS* **108**, 16545 (2011).
- [14] A. Riaz, M. Hesse, H. A. Tchelepi, and F. M. O. Jr, *J. Fluid Mech.* **548**, 87 (2006).
- [15] J. A. Neufeld, M. A. Hesse, A. Riaz, M. A. Hallworth, H. A. Tchelepi, and H. E. Huppert, *Geophys. Res. Lett.* **37**, L22404 (2010).
- [16] D. R. Hewitt, J. A. Neufeld, and J. R. Lister, *J. Fluid Mech.* **737**, 205 (2013).
- [17] M. Szulczewski, M. Hesse, and R. Juanes, *J. Fluid Mech.* **736**, 287 (2013).
- [18] A. C. Slim, *J. Fluid Mech.* **741**, 461 (2014).
- [19] Z. Shi, B. Wen, M. Hesse, T. Tsotsis, and K. Jessen, *Adv. Water Resour.* **113**, 100 (2018).
- [20] M. D. Graham and P. H. Steen, *Physica D* **54**, 331 (1992).
- [21] J. Otero, L. A. Dontcheva, H. Johnston, R. A. Worthing, A. Kurganov, G. Petrova, and C. R. Doering, *J. Fluid Mech.* **500**, 263 (2004).
- [22] D. R. Hewitt, J. A. Neufeld, and J. R. Lister, *Phys. Rev. Lett.* **108**, 224503 (2012).
- [23] D. R. Hewitt, J. A. Neufeld, and J. R. Lister, *J. Fluid Mech.* **748**, 879 (2014).
- [24] B. Wen, *Porous medium convection at large Rayleigh number: Studies of coherent structure, transport, and reduced dynamics*, Ph.D. thesis, University of New Hampshire (2015).
- [25] B. Wen, G. P. Chini, R. R. Kerswell, and C. R. Doering, *Phys. Rev. E* **92**, 043012 (2015).
- [26] D. R. Hewitt and J. R. Lister, *J. Fluid Mech.* **829**, 89 (2017).
- [27] B. Wen, L. T. Corson, and G. P. Chini, *J. Fluid Mech.* **772**, 197 (2015).
- [28] B. Wen and G. P. Chini, *J. Fluid Mech.* **837**, 670 (2018).
- [29] G. S. Pau, J. B. Bell, K. Pruess, A. S. Almgren, M. J. Lijewski, and K. Zhang, *Adv. Water Resour.* **33**, 443455 (2010).
- [30] J. Hidalgo, J. Fe, L. Cueto-Felgueroso, and R. Juanes, *Phys. Rev. Lett.* **109**, 264503 (2012).
- [31] B. Wen, N. Dianati, E. Lunasin, G. P. Chini, and C. R. Doering, *Communications in Nonlinear Science and Numerical Simulation* **17**, 2191 (2012).
- [32] B. Wen, G. P. Chini, N. Dianati, and C. R. Doering, *Phys. Lett. A* **377**, 2931 (2013).
- [33] S. Backhaus, K. Turitsyn, and R. E. Ecke, *Phys. Rev. Lett.* **106**, 104501 (2011).
- [34] Y. Liang, B. Wen, M. Hesse, and D. DiCarlo, submitted (2018).
- [35] G. de Josselin de Jong, *Transactions, American Geophysical Union* **39**, 261 (1958).
- [36] P. G. Saffman, *Journal of Fluid Mechanics* **6**, 321 (1959).
- [37] Y. Bachmat and J. Bear, *Journal of Geophysical Research* **69**, 2561 (1964).
- [38] J. Bear, *J. Geophys. Res.* **66**, 1185 (1961).
- [39] A. E. Scheidegger, *J. Geophys. Res.* **66**, 3273 (1961).
- [40] G. de Josselin de Jong and M. J. Bossen, *J. Geophys. Res.* **66**, 3623 (1961).
- [41] K. Ghesmat and J. Azaiez, *Transp. Porous Med.* **73**, 4297 (2008).
- [42] J. J. Hidalgo and J. Carrera, *J. Fluid Mech.* **640**, 441 (2009).
- [43] K. Ghesmat, H. Hassanzadeh, and J. Abedi, *AIChE J* **57**, 561 (2011).
- [44] H. Emami-Meybodi, H. Hassanzadeh, and J. Ennis-King, *Water Resour. Res.* **51**, 2595 (2015).
- [45] L. Wang, Y. Nakanishi, A. Hyodo, and T. Suekane, *Int. J. Greenh. Gas Control* **53**, 274 (2016).
- [46] T. Suekane, J. Ono, A. Hyodo, and Y. Nagatsu, *Phys. Rev. Fluids* **2**, 103902 (2017).
- [47] N. Nikitin, *Int. J. Numer. Meth. Fluids* **51**, 221 (2006).
- [48] L. W. Gelhar, C. Welty, and K. R. Rehfeldt, *Water Resources Research* **28**, 1955 (1992).
- [49] K. Johannsen, W. Kinzelbach, S. Oswald, and G. Wittum, *Advances in Water Resources* **25**, 335 (2002).
- [50] M. Muniruzzaman and M. Rolle, *Water Resources Research* **53**, 1 (2017).
- [51] S. Oswald and W. Kinzelbach, *Journal of Hydrology* **290**, 22 (2004).